Discovery of a small molecule having both potent anti-fibrotic and anti-inflammatory capabilities

Han-Soo Kim,[1,2*] Moon Kee Meang[3*], MinJu Ham[3], Ji Yong Lee,[4] Baik L. Seong[5], Ho-Sup Yoon[6], Ik-Hwan Kim,[7] and Byung-Soo Youn[3#]

[1]Department of Biomedical Sciences, Catholic Kwandong University College of Medical Convergence, Gangneung-si, Gangwon-do 25601, Republic of Korea; [2]Basic Research Division, Biomedical Institute of Mycological Resource, College of Medicine, Catholic Kwandong University, Gangneung-si, Gangwon-do 25601, Republic of Korea; [3]OsteoNeuroGenInc, Seoul, 08501, Republic of Korea; [4]Research Institute of Hyperbaric Medicine and Science, Yonsei University Wonju College of Medicine, Wonju-si, Gangwon-do 26426, Republic of Korea; [5]Department of Botechnology, Yonsei University, Seoul 03722, Republic of Korea; [6]Nanyang Technological University, Biomedical Sciences, School of Biological Sciences, 639798, Singapore and [7]Department of Biotechnology, Korea University, Seoul 02841, Republic of Korea

Running title: Chromone-Scaffold Therapeutics (CST)

*To whom contributed equally to the current investigations.

[#]To whom correspondence should be addressed: OsteoNeuroGen, Inc. Ace High-end Tower 9th 233, Gasandigital-1-ro, Geumcheon-gu, Seoul, 08501, Republic of Korea; byung4jc@gmail.com; Tel. +82-2-6267 2737; Fax. +82-2-6267-2740

Abstracts

Fibrosis is a human intractable disease. Chemicals with chromone-scaffold (CS) only was found in the plant. We found a new CS-analog, ONG41008, exhibited notable anti-fibrotic capacity. ONG41008 dismantled latent transforming growth factor complex, limiting TGFβ to TGFβ receptor. ONG41008 was able to reverse the fate of myofibroblasts into intermediated non-myofibroblasts confirmed by both cell shape changes and global transcriptomics analyses. ONG41008 inhibited induction of NADPH oxidase 4. Expression of macrophages homing chemokines was significantly mitigated. Both anti-inflammatory and anti-fibrotic capacity prompted us to investigate whether the murine NASH model (STAM mice) could be improved. ONG41008 significantly diminished nonalcoholic fatly liver disease scores. ONG41008 substantially inhibited *TNFα* and several important chemokines in the macrophages stimulated with LPS. TNFα was situated at the central hub in the LPS-ONG41008-macrophages interactome. Endocytosis of CD14, a LPS receptor, was blocked by ONG41008. ONG41008 could be a potent drug for a broad range of fibrotic diseases.

Introduction

Idiopathy pulmonary fibrosis (IPF) is defined a rare disease belonging to interstitial lung diseases (ILD).[1] Its mortality and morbidity are becoming significant such that the median survival of patients with IPF is 3~5 years after diagnosis and the majority of patients would succumb to death within 5 year of diagnosis.[2] NAFLD is becoming pandemic over the world due to overnutrition. NASH is an extreme manifestation of NAFLD associated with multiple-parallel immunometabolic dysfunctions such as steatosis, lobular inflammation or progressive fibrosis.[3, 4] It has been well appreciated that mitigation of liver fibrosis is the bottle-neck attenuating NASH.[5] Therefore, development of both potent anti-fibrotic and anti-inflammatory drugs is of paramount importance for dealing with IPF or NASH. Myofibroblasts play a central role in causing fibrosis.[6] While identification of the IPF-initiating cells remains to be discovered HSCs are the major cell types contributing to both liver inflammation and liver fibrosis.[7] Although fibrogenic signature proteins such as CTGF (connective tissue growth factor) or Periostin have been partially elucidated full spectrum of fibrogenic proteins have yet to be discovered. Nevertheless, several anti-fibrotic modalities have continually put on clinical studies.[8] Although fibrosis is not defined an immune disorder inflammatory cells are believed to be responsible for eliciting fibrogenic signaling. Among these cells macrophages including bone-marrow-derived ones and tissue residential macrophages called Kupffer cells may play important roles in establishing early stage inflammation by producing proinflammatory cytokines such as TNFα or IL-1β.[9] Therefore, controlling these proinflammatory cytokines may lead to an efficient modality for fibrotic diseases.

Flavones are members of the polyphenol family, a group of >10,000 compounds predominantly found in the plant kingdom.[10] In general, these phytochemicals protect plants from radiation damage.[11] Due to their anti-oxidant and anti-inflammatory potentials, flavones

have long been used to treat inflammatory diseases such as arthritis and asthma.[12] Chromone, 1,4-benzopyrone-4-one, is a central chemical scaffold constituting flavones,[13] and the chromone derivatives (CDS) are a diverse family based on branching chemical residues coupled to this core chemical framework.[14] We recently reported that eupatilin, a CD from an *Artemisia* species, dramatically inhibits LPS-induced osteoclastogenesis via actin depolymerization[15] and downregulation of multiple genes associated with EMT. Here, we show that a noble CD called ONG41008 is able to reprogram EMT and induce reversion of pathogenic myofibroblasts to intermediate non-myofibroblasts, likely ameliorating lung fibrosis.[16] In addition to this, ONG41008 blocks LPS-induced macrophage activation via interacting with CD14, independently of TGFβ. This observation opens a door as a powerful new therapeutic modality for treating IPF as well as liver fibrosis or autoreactive T cells-mediated hyper-inflammation.

Results

Toxicity and DMPK study on ONG41008

Non-GLP (Good Laboratory Practice) toxicokinetic studies using rats told us that ONG41008 existed in plasma over 12 hr via oral administration, resulting in T*max* (1~2hr) and (260.8ng ± 41.4ng) as seen in supplementary (S1A). A 14 Days' oral gavage toxicity assessment rendered non-toxic. The same held true for non-GLP single injection oral PK study using beagle dogs (S1B). Mice and rats were subjected to tissue PK studies within 2hr upon oral administration. As seen in S2, ONG41008 was largely detected within 30 min from plasma, lung, liver or kidney tissues of mice or rats.

ONG41008 dismantles latent TGF complex (LTC) via depolymerization of F-actin.

When ONGHEPA1(a mouse hepatic stellate cell line) or DHLFs (diseased human lung fibroblasts) were stimulated with TGFβ expression of α-smooth muscle actinin (αSMA) was notable but was then substantially mitigated with the treatment of ONG41008 (Figure 1A and 1B). Likewise, other fibrinogenic markers involving C*ollagen11α1*, C*ollagen1α1* and *Periostin or Aurora kinase (AURKA)* was induced by TGFβ and was knocked down by ONG41008, suggesting that ONG41008 may directly act on pathogenic myofibroblasts both in the lung or liver fibrotic tissues. ONG41008 markedly inhibited phosphorylation of both SMAD2 and SMAD3 not ERK, suggesting that phosphorylated Smad2 and/or Smad3 may translocate to the nucleus, activating fibrogenesis phosphorylation of ERK was vibrant remained unknown. We know ONG41008 itself is unable to phosphorylate ERK.

As shown in our previous study, eupatilin was able to depolymerize F-actin. Thus, we hypothesized that F-actin in actin stress fibers may be also a molecular target for ONG41008. As shown in Figure 1D, actin stress fibers appeared to be dense at focal adhesion regions. While massive actin depolymerization was observed with the treatment of ONG41008 no such

depolymerization was seen in ONGHEAPA1 cells stimulated with pirfenidone or nintedanib, suggesting that the latter two anti-IPF drugs may have no effects on F-actin depolymerization. *In vitro* actinpolymerization or depolymerization assay was established and showed that ONG41008 was an inhibitor of actin polymerization (Figure 1E) as well as an enhancer of actin depolymerization (Figure 1F). It is well appreciated that osteoclasts exist as fused state whereby O-ring made of F-actin surrounds fused osteoclasts called multinucleated osteoclasts.[17] As shown in S3, ONG41008-treated multinucleated osteoclasts tremendously gave rise to actin fragments. These studies indicate that ONG41008 is a bona-fide F-actin depolymerizer.

To further elucidate mode of action (MOA) for ONG41008, we stimulated DHLFs with TGFβ plus ONG41008 and stained them with various antibodies recognizing the components of LTC. LTC plays a central role of TGFβ biogenesis,[18] releasing active TGFβ, which is later on engaged in TGFRII, giving rise to phosphorylation of SMAD2/SMAD3. Among the known components, LTBP1 and LAP1 were tremendously induced and secreted into the extra cellular matrix (ECM) compartments with the treatment of TGFβ, but unexpectedly, LTBP4 appears to be either only partially affected or unaffected by ONG41008 (Figure 1G). ONGHEPA1 cells were also treated with TGFβ in the presence or absence of ONG41008 for 24 hr. It is evident that LTBP1, LAP1 and Integrin α5β3 in the presence of ONG41008 were massively downregulated and seemed to be situated in endosome-like vesicles and actin stress fibers significantly were disappeared (Figure 1H).

Generation of ONG41008-mediated fibrogenic interactome and identification of NOX4 as an anti-inflammatory component in lung and liver fibrosis.

In order to identify the ONG41008-suppressible fibrosis-inducing genes (FIGS), DHLFs were differentially stimulated with TGFβ in the presence or absence of ONG41008

and transcriptomic change was analyzed by RNA-seq. Schematic representation of this selection process is shown in S4. We nailed down seventy-seven ONG4108-suppressible FIGS with p>0.005 in DHFLs. Many of those genes have been already known to be fibrogenic such as CTGF, PERIOSTIN, LOX, or CDH2.[19, 20, 21] Among those, NOX4, a NADPH oxidase, caught our attention because induction of NOX4 has been reported for production of pronounced reactive oxygen species (ROS) as well as for elicitation of several important signaling events like LPS signaling or inflammasome activation.[22] This data suggests that NOX4 plays an important role in pathogenesis of myofibroblasts. According to an interactome analysis, NOX4 seemed to be functionally related to endothelin (EDN) 1, connective tissue growth factor (CTGF) and insulin-like growth factor binding proteins (IGFBP)3 (S4). HSCs play a pivotal role in hepatic inflammation as well as liver fibrosis.[23, 24] To scrutinize whether ONG41008 is able to suppress induction of *NOX4*, thereby downregulating ROS production, ONGHEPA1 cells were stimulated with TGFβ and induction kinetics of *NOX4* along with some fibrogenic genes were analyzed at transcription and protein levels. As shown in Figure 2A, N*ox4* mRNA and NOX4 polypeptide were significantly induced by TGFβ and ONG41008 was able to block the induction, suggesting that ONG41008 is an inhibitor of *NOX4* inducer. Production of ROS was also significantly attenuated, which is shown by immunocytochemistry (ICC) (Figure 2B). The same held true for DHLFs (Figure 2C). Furthermore, ROS production was markedly reduced via ROS dye staining (Figure 2D). ONG41008 was able to block the induction of *NOX4*, *CCL2* and *CCL7* (Figure 2E), suggesting that ONG41008 could modulate migration of macrophages to the liver.

ONG41008 is a potent inducer of autophagy independently of TGFβ

It has been appreciated that autophagy plays a pivotal role in attenuating fibrosis.[25, 26] To see if ONG41008 is able to form autophagosomes DHLFs or ONGHEPA1 cells were treated with TGFβ plus ONG41008. Complete inhibition of fibrosis as well as autophagosomes

were clearly noted (Figure 3A). ONGHEPA1 cell lysates were subjected to western blot with the use of a cleavage-specific anti-LC3. The fragmentation of LC3 protein, becoming the A/B polypeptide fragments, was apparent when treated with TGFβ. Serum starvation might accelerate this autophagy induction. However, ONG41008 plus TGFβ gave rise to substantial increase in LC3A/B (Figure 3B). ICC was performed with anti-p62 or anti-LC3 (Figure 3C and 3D). P62 also called seqestsome is normally found at the nucleus as aggregated forms.[27] Upon contact with ONG41008 without TGFβ a vast fraction of P62 was distributed the lysosomal compartments. The same held true that robust induction of LC3 A/B was notable with ONG41008 only. The ONG4100-mediated autophagy formation is TGFβ-independent. Taken together, this data shows that ONG41008 is a potent anti-inflammatory drug coupled with intrinsic autophagy induction that might lessen disease severities associated with IPF, liver inflammation in NASH or liver fibrosis.

ONG41008 mediates cell reversion.

During the course of this study it has occurred to our attention that ONG41008 treatment alone reversed the cell fate of pathogenic myofibroblasts into intermediate non-pathogenic cell types. To have a deeper understanding on this reversion mechanism we established a series of continual differentiation stages in such a way that morphological changes as well as interactome changes were closely monitored. As shown Figure 4A, trans-differentiation was set aside by stimulating ONGHEPA1 cells with TGFβ for 24hr after which the resultant myofibroblasts were washed off with buffer and were subjected to TGFβ plus ONG41008 or ONG41008 alone (data not shown) for 48hr because the combinatorial treatment seemed to be more pertinent to *in vivo* situation. The treated cells were re-plated out and continually were stimulated with TGFβ alone for 72hr. Upon complete trans-differentiation stimulation of myofibroblasts with TGFβ plus ONG41008 remarkably transformed

myofibroblasts into intermediate cells. Moreover, these intermediate cells seemed to be in quiescence since no cell growth was observed. We extended our question to see if these quiescent cells can be trans-differentiated with the treatment of TGFβ alone. We discovered that trans-differentiation resumed at least 48hr after TGFβ stimulation, suggesting that this reversion process should be a flexible differentiation program *in vitro*. To determine if this remarkable reversion process has to do with nuclear reprogramming, we extensively analyzed global gene expression changes at each stimulation condition. As shown in Figure 4B, a hybrid interactomes existed in the reversion process; 1) fibrogenic interactome and 2) reversion interactome. The latter one is apparently composed of residual fibrogenic interactome and nuclear reprograming one. ONG41008 is able to generate intermediate cells based on a hybrid interactome. Figure 5 demonstrates two distinct anti-fibrotic capacities associated with ONG41008; 1) inhibition of TGFβ biogenesis by dismantling of LTC via F-actin depolymerization, thereby limiting binding of TGFβ to TGFRII and 2) alteration of ECM biogenesis which is initiated in currently unknown modes but TGFβ-independent autophagy formation and reversion of myofibroblasts into intermediate cells are remarkable features associated with ONG41008.

In vivo therapeutic efficacy of ONG41008 for anti-IPF

Therapeutic efficacy of IPF was analyzed via mouse bleomycin lung fibrosis model (BLM) (Figure. 6). For prevention model, oral administration of a range of 10 to 50mpk ONG41008 was used. ONG41008 at 10mpk or 25mpk effectively blocked production of soluble collagen with statistical significance as shown in S5A whereas no statistical significance at 50mpk was shown. On the contrary, since 50mpk exhibited the most effective inhibitory capacity on hydroxyproline production the used mice colony might not properly respond to BLM (S5A). Pirfenidone only gave rise to decreasing tendencies in reduction of

soluble collagen or HP production. Masson-Trichome tissue staining was conducted as shown in S5B. Apparently, ONG41008 at three administration concentrations remarkably reduced collagen deposition whereas dexamethasone was unable to improve the disease severity. We also found that pirfenidone at 100mpk or ONG41008 at 100mpk consistently inhibited *in vivo* TGFβ production (S10). Therapeutic BLM model was also performed in which bleomycin had been intrathecally administered for 1 week followed by daily oral administration of ONG41008 for 2 weeks. A greatest reduction in collagen production was observed at ONG41008 50 or 100mpk, whereas no significant inhibition was noted at ONG41008 10mpk as well as at pirfenidone 100mpk unlike the above prevention model, suggesting that larger exposure of ONG41008 may be needed to cope with existing lung fibrosis in therapeutic model. While production of HP at 10mpk and 50mpk of ONG41008 only exhibited reduction tendency 100mpk remarkably inhibited HP production with a statistical significance (Figure 6A). Expression of αSMA were more significantly decreased in those ONG41008-treated mice than control mice. However, dexamethasone did not affect αSMA staining, indicating that anti-inflammation may not be able to mitigate proliferation of myofibroblasts at advanced stages (Figure 6B). Taken together, ONG41008 could be a good candidate for treating IPF as a monotherapy or as a combination therapy with pirfenidone.

In vivo therapeutic efficacy of ONG41008 for anti-NASH

We supposed that these combined anti-inflammatory and anti-fibrotic capabilities associated with ONG41008 may make ONG41008 an ideal drug for NASH. NASH is characterized by fatty liver, lobular inflammation, hepatocyte ballooning and progressive fibrosis.[4] Due to these multifaceted clinical features, NASH has become a most-challenging immunometabolic aillment.[28] Blockade of either inflammation or/and fibrosis may be able to ameliorate NASH. We adapted the STAM mouse model in which five to eight weeks STAM

mice exhibit the most human resembling NASH.[29] STAM mice were orally administered with vehicle, ONG41008 50mpk, Telmisartan 30mpk (positive control) or obeticholic acid (OCA) 30mpk as negative control. ONG41008 50mpk gave rise to a clear sign of improvement of fatty liver as seen in Figure 6C whereas no improvement of NASH was noted at OCA 30mpk. There were decreasing trends in lobular inflammation and hepatocyte ballooning by ONG41008 50mpk and little degree of inhibition of fibrosis was also noted with the treatment of OCA 30mpk (data not shown). Telmisartan showed clear improvement in all score parameters (Figure 6D). Pathologic manifestation was scored as shown in Figure 6E; 1) steatosis, 2) lobular inflammation and 3) hepatocyte ballooning as well as hepatic fibrosis. Close pathological examination revealed that ONG41008 and telmisartan are therapeutically effective for NASH based on NAFLD scores (Figure 6F).

ONG41008 is a potent inhibitor of innate immunity in that it could be a TNFα antagonist in macrophages independently of TGFβ

It has been lately reported that knocking out *TNFα* negatively affects steatosis or NFALD score.[30] Since we only explored a potent anti-inflammatory capability associated with ONG41008 in HSCs or DHLFs in TGFβ-dependent manner a natural question would be whether its anti-inflammatory property can be extended to macrophages in response to LPS stimulation in the absence of TGFβ. RAW264.7 cells, a mouse monocytic leukemic cell line resembling macrophages, were stimulated with LPS in the presence or absence of ONG41008. As shown in Figure 7A, expression of proinflammatory cytokines or chemokines involving *TNFα*, *CCL2*, *CCL7*, *CXCL2* and *CXCL10* were markedly downregulated. Interestingly, *CHOP* or *NOX1* was so markedly reduced (data partially shown) that formation of inflammasome could be attenuated.[31, 32, 33] However, no statistically significant repression of *IL6* or *IL23* was made (data not shown). TNFα ELISA was such conducted that TNFα protein

levels were clearly reduced (S6). Varying LPS concentrations (100ng/ml to 10μg/ml) showed that ONG41008 effectively blocked expression of *TNFα*, suggesting that some membrane proximal events might be responsible for the ONG41008-mediated inhibition of *TNFα* gene expression (S6). It strongly indicates that ONG41008 may inhibit formation of TLR4-LPS binding proteome or signalosome such as CD14, MD-2 or Myd88.[34] This prompted us to explore intracellular trafficking of these proteins upon LPS stimulation. As shown Figure 7B, CD14 and Myd88 exhibit endocytosis by LPS but were redistributed in plasma membrane when the cells were treated with ONG41008 via confocal imaging. Magnified views on these ICC further clearly revealed the relocation of CD14 to plasma membrane (S7). On the contrary, MD-2 and NOX4 remained unaltered (S8). An interactome operating for LPS-ONG41008 axis in macrophages. To our surprise, TNFα turned out to be the central hub of the interactome, strongly suggesting that ONG41008 may be a TNFα antagonist (Figure 7C). Summing up all these observations we believe that ONG41008 is an endocytosis inhibitor of CD14, remarkably diminishing macrophage activation. This is schematically represented in S9. It should be stressed here that ONG41008 is intrinsically equipped with both anti-inflammatory and anti-fibrotic capabilities, indicating that its applicability could well suit immunometabolic dysfunctions or controlling innate immunity.

Discussion

Chromone-scaffold derivatives (CSD) have been well appreciated for their anti-inflammation capabilities.[35] We recently found that a few CSD are capable of attenuating *in vitro* and *in vivo* fibrosis.[36] Slight modification of functional groups linked to CSD severely affected degree of anti-fibrosis, suggesting that medicinal chemistry would be able to improve their therapeutic efficacy. One drawback associated with CSD in terms of *in vivo* use for treating fibrosis is that CSD administered into rodents largely undergoes glucuronidation. We confirmed that this chemical modification completely impaired the anti-fibrotic capacity of CSD. Thus, development of the analogs coping with this impairment should have been implemented. ONG41008 rendered non-toxic when subjected to non-GLP toxicity. PK profiles using rats or beagle dogs via oral administration were readily detectable. In many senses, ONG41008 could be a therapeutically pertinent drug candidate.

The major MOA seems to dismantle LTC in such a way that ONG41008 limits binding of TGFβ to TGFR; one major manifestation is blocking phosphorylation of SMAD2/SMAD3, resulting in disabling type 2 EMT so called fibrogenesis. However, phosphorylation of ERK was not affected by ONG41008, suggesting that ONG41008 is largely associated with the main signaling of TGFR, i.e. phosphorylation of SMAD2/SMAD3. We demonstrated that ONG41008 was able to reverse the cell fate of pathogenic myofibroblasts into intermediate non-pathogenic myofibroblasts. This reversion process did not seem to require TGFβ. Continual stimulation with TGFβ over 72hr enabled the intermediated cell types to be transdifferentiated into myofibroblasts, suggesting that ONG41008-mediated reversion may be an *in vitro* flexible differentiation program. Consistently with generation of a hybrid interactome, the reversion process may be controlled at chromatin levels. In particular, it has been noted that this sort of intermediated cell types is often observed from the biopsy samples of the liver cirrhosis patients.[37] Our *in vitro* demonstration that two distinct interactomes,

fibrogenic interactome and nuclear interactome, coexist in the ONG41008-treated myofibroblasts supports the observation. Nevertheless, how ONG41008 initiates this reversion process remains to be determined in order to discover a molecular target for a central role by ONG41008.

Autophagy plays a central role in IPF or liver diseases such as steatosis or liver fibrosis. Like the reversion process associated with ONG41008 redistribution of p62 into lysosomal compartments or LC3 fragmentation is also TGFβ-independent, suggesting that ONG41008 may be equipped with its intrinsic capability modulating an array of cell physiology. Since the degree of lysosomal trafficking of p62 via ONG41008 was significant comparison with mTORC1 signaling or its upstream signaling such as PI3k, PDK and Akt axis should be investigated. With the use of DART (Direct Analysis in Real Time) discovery of a molecular target(s) existing ECM would desirable. Crucial role of TNFα associated with liver diseases prompted us to scrutinize effect of ONG41008 on macrophage physiology. As macrophages play a central role in inflammation whose activation has been known to be modulated by ROS[38] and ONG41008 mitigated *NOX4* gene expression in DHLFs, how ONG41008 regulates *NOX4* gene expression in ONGHEPA1 cells remains intriguing. As anticipated, ONG41008 was able to greatly attenuate *NOX4* transcription along with *Collagen11α1* or *Periostin*. Furthermore, knocking down *NOX4* transcription by ONG41008 mirrored downregulation of macrophages-chemoattractant proteins such as *CCL2* and *CCL7*, suggesting that ONG41008 may affect macrophage homing to the liver. Macrophage infiltration is pathologically related to steatosis or liver inflammation.[39] ONG41008 seemed to be able to compete for binding to CD14, a LPS receptor, and inhibit endocytosis of CD14 or Myd88, disarming TLR4-driven TNFα production. Although our confocal imaging analysis may set a working hypothesis that ONG4100 directly bind to CD14, more analytical interaction studies should be performed like DART. ICC data clearly showed that LPS stimulation robust endocytosis CD14 whereas LPS

plus ONG41008 may retain periplasmic distribution of CD14 in conjunction with remarkable morphological change showing round shapes (S7). How ONG41008-mediated morphological change occurred and this morphological change affects LPS-mediated TNFα induction remains to be elucidated. No apparent change in endocytosis and morphological changes of MD-2 or NOX4 were detected (S8). LPS-LBP is supposed to bind to a COOH-terminal region of CD14. Formation of these trimeric complex may directly prevent the endocytosis of CD14 whereas MD-2-TLR4 complex does not seem to be redistributed in the LPS-stimulated RAW264.7 cells.

We performed a series of lung tissue PKs to see how much parental compounds remain 1hr after oral administration. As shown in S10. Compared to pirfenidone at 100mpk the accumulated ONG41008 was around tenfold less than that of pirfenidone, suggesting that disease-correcting signaling associated with a given drug may be more relevant index for therapeutic efficacy than bioavailability. We have currently succeeded in selecting salt forms fitting to ONG41008. Polymorph selection is undergoing. Hopefully, these modification efforts may create a high bioavailability.

Taken together, we discovered a CS-containing small molecule called ONG41008 that has both anti-fibrotic and anti-inflammatory capability. ONG41008 may be able to ameliorate a broad range of fibrosis such as heart fibrosis, kidney fibrosis, macular fibrosis, NASH or fibrotic cancers such as pancreatic cancer. This observation also opens a door as a powerful new therapeutic modality for treating autoreactive T cells-mediated hyper-inflammation.

Acknowledgments

This study was supported by an intramural fund from OsteoNeuroGen.

Competing financial interests

H-S Kim, I-K Kim, and B-S Youn retain shares of OsteoNeuroGen, and M-K Meang and MJ Ham are employed by OsteoNeuroGen. The current contents of the ONG41008 data has been granted, as the subject of a Korean patent and a US patent has been subjected to USPTO.

Author contributions

B-S Youn and H-S Kim conceived the idea. I-H Kim and B L. Seong coordinated the experiments and helped to write the manuscript. M-K Meang, MJ Ham and JY Lee were largely involved in executing major experiments,

Animal care: Mice, rats or beagle dog care was managed by the IACUC associated with Syngene International (Bangalore, India).

Footnotes:

The following abbreviated terms were mainly used in this manuscript;

CS: Chromone Scaffold

CSD: Chromone Scaffold Derivatives

IPF: Idiopathy Pulmonary Fibrosis

BLM: Bleomycin-Induced Lung Fibrosis

NASH:Non-Alcoholic Steato Hepatitis

DHLFs: Diseased Human Lung Fibroblasts

LTC: Latent TGF Complex

References

1. Meyer KC. Pulmonary fibrosis, part I: epidemiology, pathogenesis, and diagnosis. *Expert Rev Respir Med* **11**, 343-359 (2017).

2. Raghu G*, et al.* Idiopathic Pulmonary Fibrosis: Prospective, Case-Controlled Study of Natural History and Circulating Biomarkers. *Chest* **154**, 1359-1370 (2018).

3. Wattacheril J, Issa D, Sanyal A. Nonalcoholic steatohepatitis (NASH) and hepatic fibrosis: Emerging therapies. *Ann Rev Pharmacol Toxicol* **58**, 649-662 (2018).

4. Bessone F, Razori MV, Roma MG. Molecular pathways of nonalcoholic fatty liver disease development and progression. *Cell Mol Life Sci* **76**, 99-128 (2019).

5. Marra F, Lotersztajn S. Pathophysiology of NASH: perspectives for a targeted treatment. *Curr Pharm Des* **19**, 5250--5269 (2013).

6. Kramann R, Schneider RK. The identification of fibrosis-driving myofibroblast precursors reveals new therapeutic avenues in myelofibrosis. *Blood* **131**, 2111-2119 (2018).

7. Ignat SR, Dinescu S, Hermenean A, Costache M. Cellular interplay as a consequence of inflammatory signals leading to liver fibrosis development. *Cells* **9**, E461 (2020).

8. Lemoinne S, Friedman SL. New and emerging anti-fibrotic therapeutics entering or already in clinical trials in chronic liver diseases. *Curr Opin Pharmacol* **49**, 60-70 (2019).

9. Miao CM*, et al.* Bone marrow stromal cells attenuate LPS-induced mouse acute liver injury via the prostaglandin E 2-dependent repression of the NLRP3 inflammasome in Kupffer cells. *Immunol Lett* **179**, 102-113 (2016).

10. Dixon RA, Pasinetti GM. Flavonoids and isoflavonoids: From plant biology to agriculture and neuroscience. *Plant Physiol* **154**, 453-457 (2010).

11. Stapleton AE, Walbot V. Flavonoids can protect maize DNA from the induction of ultraviolet radiation damage. *Plant Physiol* **105**, 881-889 (1994).

12. Leyva-López N, Gutierrez-Grijalva EP, Ambriz-Perez DL, Heredia JB. Flavonoids as cytokine modulators: A possible therapy for inflammation-related diseases. *Int J Mol Sci* **17**, 921 (2016).

13. Emami S, Ghanbarimasir Z. Recent advances of chroman-4-one derivatives: synthetic

approaches and bioactivities. *Eur J Med Chem* **93**, 539-563 (2015).

14. Gacche RN, *et al.* Flavonoids as a scaffold for development of novel anti-angiogenic agents: An experimental and computational enquiry. *Arch Biochem Biophys* **577-578**, 35=48 (2015).

15. Kim JY, Lee MS, Baek JM, Park J, Youn BS, Oh J. Massive elimination of multinucleated osteoclasts by eupatilin is due to dual inhibition of transcription and cytoskeletal rearrangement. *Bone Rep* **3**, 83-94 (2015).

16. Troeger JS, *et al.* Deactivation of hepatic stellate cells during liver fibrosis resolution in mice. *Gastroenterology* **143**, 1073-1083 (2012).

17. Wang Y, *et al.* Role of actin filaments in fusopod formation and osteoclastogenesis. *Biochim Biophys Acta* **1853**, 1715-1724 (2015).

18. Robertson IB, Horiguchi M, Zilberberg L, Dabovic B, Hadjiolova K, Rifkin DB. Latent TGF-β-binding proteins. *Matrix Biol* **47**, 44-53 (2015).

19. Makarev E, *et al.* Common pathway signature in lung and liver fibrosis. *Cell Cycle* **15**, 1667-1673 (2016).

20. Wang Y, Yella J, Chen J, McCormack FX, Madala SK, Jegga AG. Unsupervised gene expression analysis identify IPF-severity correlated signatures, associated genes and biomarkers. *BMC Pulm Med* **17**, 133 (2017).

21. Mullenbrock S, *et al.* Systems analysis of transcriptomic and proteomic profiles identifies novel regulation of fibrotic programs by miRNAs in pulmonary fibrosis fibroblasts. *Genes (Basel)* **9**, pii: E588 (2018).

22. Singh A, *et al.* NADPH oxidase 4 modulates hepatic responses to lipopolysaccharide mediated by Toll-like receptor-4. *Sci Rep* **7**, 14346 (2017).

23. Weiskirchen R, Tacke F. Cellular and molecular functions of hepatic stellate cells in inflammatory responses and liver immunology. *Hepatobiliary Surg Nutr* **3**, 344-363 (2014).

24. Higashi T, Friedman SL, Hoshida Y. Hepatic stellate cells as key target in liver fibrosis. *Adv Drug Deliv Rev* **121**, 27-42 (2017).

25. Liu T, *et al.* Alleviation of hepatic fibrosis and autophagy via inhibition of transforming growth factor-β1/Smads pathway through shikonin. *J Gastroenterol Hepatol* **34**, 263-

276 (2019).

26. Hill C, *et al.* Autophagy inhibition-mediated epithelial-mesenchymal transition augments local myofibroblast differentiation in pulmonary fibrosis. *Cell Death Dis* **10**, 591 (2019).

27. Fan W, *et al.* Keap1 facilitates p62-mediated ubiquitin aggregate clearance via autophagy. *Autophagy* **6**, 614-621 (2015).

28. Monteiro PA, do Prado WL, Dos Santos Tenório TR, Tomaz LM, St-Pierre DH, Lira FS. Immunometabolic Changes in Hepatocytes Arising from Obesity and the Practice of Physical Exercise. *Curr Pharm Des* **24**, 3200-3209 (2018).

29. Saito K, *et al.* Characterization of hepatic lipid profiles in a mouse model with nonalcoholic steatohepatitis and subsequent fibrosis. *Sci Rep* **5**, 12466 (2015).

30. Kakino S, *et al.* Pivotal role of TNF-α in the development and progression of nonalcoholic fatty liver disease in a murine model. *Horm Metab Res* **50**, 80-87 (2018).

31. Grant R, Nguyen KY, Ravussin A, Albarado D, Youm YH, Dixit VD. Inactivation of C/ebp homologous protein-driven immune-metabolic interactions exacerbate obesity and adipose tissue leukocytosis. *J Biol Chem* **289**, 14045-14055 (2014).

32. Sun B, *et al.* NADPH Oxidase-Dependent NLRP3 Inflammasome activation and its important role in lung fibrosis by multiwalled carbon nanotubes. *Small* **11**, 2087-2097 (2015).

33. Zhang LL, *et al.* Angiotensin(1-7) attenuated Angiotensin II-induced hepatocyte EMT by inhibiting NOX-derived H2O2-activated NLRP3 inflammasome/IL-1β/Smad circuit. *Free Radic Biol Med* **97**, 531-543 (2016).

34. Cheng Z, Taylor B, Ourthiague DR, Hoffmann A. Distinct single-cell signaling characteristics are conferred by the MyD88 and TRIF pathways during TLR4 activation. *Science Signaling* **8**, ra69 (2015).

35. Owona BA, Abia WA, Moundipa PF. Natural compounds flavonoids as modulators of inflammasomes in chronic diseases. *Int Immunopharmacol* **84**, 106498 (2020).

36. Kim HS, *et al.* Reversion of in vivo fibrogenesis by novel chromone scaffolds. *EBioMedicine* **39**, 484-496 (2019).

37. Karin D, Koyama Y, Brenner D, Kisseleva T. The characteristics of activated portal

fibroblasts/myofibroblasts in liver fibrosis. *Differentiation* **92**, 84-92 (2016).

38. Nonnenmacher Y, Hiller K. Biochemistry of proinflammatory macrophage activation. *Cell Mol Life Sci* **75**, 2093-2109 (2018).

39. Koyama Y, Brenner DA. Liver inflammation and fibrosis. *J Clin Invest* **127**, 55-64 (2017).

Figure legends

Fig. 1. ONG41008 inhibits trans-differentiation of human lung fibroblast or murine hepatic stellate cells into myofibroblasts. (A) ICC was performed for α-SMA on ONGHEPA1 and (B) DHLF after 24hrs treatment with medium, TGFβ, TGFβ plus ONG41008, and was observed under florescent microscope. Periostin, Collagen1α1, Collagen11α1, and AURKA mRNA level was measured by qPCR in parallel to ICC set. (C) Kinetics of ONG41008 induced SMAD and ERK phosphorylation in presence of TGFβ. Western blot of ONGHEPA1 treated with TGFβ, and with ONG41008 was taken at time period of 0, 5, 15, 30, 45, 60, 120 mins. (D) Actin-Phalloidin staining to test actin depolymerization. In presence of TGFβ, ONG41008, Pirfenidone, or Nintedanib was treated on DHLF and observed under microscope. (E) *In vitro* actin polymerization and (F) depolymerization assay. Actin polymerization activity and amount of depolymerization was measured in kinetic mode fluorometer at different concentration of ONG41008. Statistical significance was calculated by Student's t-test. *, $P < 0.05$, **, $P<0.01$. ICC was also performed for detection of latent complex proteins in (G) DHLF and (H) ONGHEPA1, along with an additional phalloidin staining for ONGHEPA1.

Fig. 2. NOX4, CCL2 and CCL7 are inducible by TGFβ and blocked by ONG41008. (A) qPCR for TGFβ treated ONGHEPA1 at timepoint 0, 6, 9, 12, 24 hr for *Collagen11α1, Periostin* and *NOX4*. (B) ICC for NOX4 on ONGHEPA1 and (C) DHLF incubated 24hrs in medium, TGFβ, TGFβ plus ONG41008. With the same treatment conditions, (D) ROS assay using DCFDA on ONGHEPA1 and (E) qPCR for *NOX4, CCL2, CCL7* on ONGHEPA1 was performed.

Fig. 3. ONG41008 induces formation of autophagosome in both DHLF and ONGHEPA1. (A) During ICC staining for ONGHEPA1 and DHLF small granular stains were observed on TGFβ plus ONG41008 samples but not on TGFβ samples. (B) ONGHEPA1 cells were treated with TGFβ or ONG41008 or TGFβ plus ONG41008 and harvested for western blotting at time point of 0, 5, 15, 30, 45, 60, 120 mins. Samples were blotted for autophagy markers LC3 A/B and P62.

Fig.4. ONG41008 reverses myofibroblasts into intermediate non-myofibroblasts. (A) Trans-differentiation was conducted for 24 hr. Myofibroblasts were washed with buffer and were restimulated with TGFβ plus ONG41008 for 24 hr. And the resultant cells, intermediate cells, were kept incubated with TGFβ alone for 72 hr. Morphological changes were monitored under a phase-contrast microscope. (B) Fibrogenic interactome in ONGHEPA1was acquired by differential stimulations; medium, TGFβ or TGFβ plus ONG41008. Collagen hubs, cell adhesins hubs and chemokines hubs are denoted by arrows. Fibogenic Spp1 protein is denoted by a blue box. Intermediate cells were subjected to RNA-seq for establishing reversion interactome and two distinct interactome coexist; 1) residual fibrogenic interactome comprising Col6a3, Col11α1 and Spp1 and 2) nuclear reprogramming interactome came evident.

Fig. 5. Mode of action of ONG41008. Major one destroys actin stress filaments via depolymerization of F-actin, leaving latent TGFβ complex dismantled. Inability of TGFβ binding to TGFβ II or I signaling receptor is unable to generate canonical or noncanonical TGFR signaling leading to attenuation of type 2 EMT. Furthermore, ONG41008 blocks phosphorylation of SMAD 2/3. These two acting mechanisms may be responsible for

efficiently disarming proliferation of or collagen or hydroxyproline production of myofibroblasts. Reversion and induction of autophagy independently of TGFβ may play an important role in giving rise to beneficial features, suggesting that it may also prevent fibrosis and promote cellular homeostasis such as cell survival, anti-steatosis or lowering insulin resistance. We suppose that these two working mechanism might be initiated from ECM.

Fig. 6. ONG41008 showed positive effect against lung fibrosis in both BLM prevention and therapeutic model. ONG41008 showed positive effect against NASH and NAFLD in STAM mouse model. (A) Lung collagen and hydroxyproline levels were measured after pirfenidone or different dosages of ONG41008 (10, 25, 50 mpk) in BLM prevention model (S5) and BLM therapeutic model. Percent inhibition relative to Vehicle control are presented in blue characters, with average measurement in black. (B) Lung sections were analyzed by Masson's Trichome staining for BLM prevention model and αSMA staining was conducted. Statistical significance was calculated by Student's t-test. ***, $P < 0.001$, relative to Sham. $, $P < 0.05$, $$$, $P < 0.001$ relative to vehicle control. (C-D) H&E staining of liver sections of STAM mouse were analyzed after Telmisartan, OCA or ONG41008. Liver samples were photographed after hepatectomy. (E) Signs of hepatic steatosis, lobular inflammation and hepatocyte ballooning in each condition were sorted by score. (F) NAFLD activity score charted for ONG41008 and controls. Statistical significance was calculated by Student's t-test.

Fig. 7. Inhibition of LPS activated genes by ONG41008 in RAW264.7 cell and ONG41008 could be an endocytosis inhibitor of CD14 and a TNFα antagonists. (A) RAW264.7 cells were stimulated with LPS (100ng/ml) or LPS plus ONG41008 (25μM, 50μM) for 24hrs and mRNA expression for inflammatory markers were measured by qPCR. (B) Confocal imaging analysis for CD14 in RAW264.7 cells were incubated in medium, LPS or

LPS plus ONG41008. CD14 or Myd66 cellular trafficking was monitored via confocal imaging. (C) An interactome operating for LPS-ONG41008 axis in macrophages TNFα turned out to be the central hub of the interactome.

Materials and Methods

Cell culture and reagents

DHLFs were purchased from Lonza (Basel, Switzerland) and cultured in fibroblast growth medium (FBM, Lonza, Walkersville, MD, USA). Recombinant human TGF-β and PDGF were obtained from Peprotech (Rocky Hill, CT, USA) and used at a final concentration of 5 ng/ml. Chemically synthesized ONG41008 was obtained from Syngene International Ltd. (Bangalore, India), dissolved at a stock concentration of 50 mM in DMSO, and stored in aliquots at -20°C. DMSO with according concentration was used as control. RAW264.7 cell line was purchased from Korean Cell Line Bank (Seoul, Korea) and cultured in RPMI supplemented with 10% FBS and 1% P/S (Welgene, Seoul, Korea). LPS was purchased from Sigma and used at final concentration of 100 ng/ml.

Effects of drugs on bleomycin-induced lung tissue fibrosis

C57BL/6J mice were anesthetized by inhalation of 70% N_2O and 30% O_2 gas containing 1.5% isoflurane. Fifty microliters of bleomycin solution in distilled water was directly injected into the lungs, all at once, via the aperture. Immediately after injection, the mice were allowed to recover from the anesthetic, and then housed in normal cages. Bleomycin (0.03U BLM in 50μl saline) was administered once using a visual instillobot. Twelve days after the administration of bleomycin, ONG41008 was forcibly nasally administered via a micropipette, once a day (five times a week) for 1 week. ONG41008 was dissolved in DPBS buffer (containing 1% DMSO), and 1 ml/kg was administered based on the most recent body weight. For 2 to 3 days after administration of ONG41008, mice were monitored for toxic symptoms or death, but no abnormal symptoms were observed. Three mice per test group were selected, and their lung tissues were excised. The lung tissues were

stained with Masson's trichrome and observed under a microscope. Results were expressed as mean values and standard deviations. One hour before sacrifice, a final dose of ONG41008 or pirfenidone was administered for plasma or lung PK. The bleomycin-treated mice exhibited a rapid decline in weight, but the sham control behaved normally. ONG41008- or pirfenidone-administered mice exhibited weight gain from day 3 onward. Control and ONG41008-treated mice data were compared using Student's *t*-test. "Differences between samples were considered statistically significant when $p<0.05$.

RNA-seq processing, differential gene expression analysis, and interactome analysis

Processed reads were mapped to the *Mus musculus* reference genome (Ensembl 77) using Tophat and Cufflink with default parameters. Differential analysis was performed using Cuffdiff using default parameters. Further, FPKM values from Cuffdiff were normalized and quantitated using the R Package Tag Count Comparison (TCC) to determine statistical significance (e.g., P values) and differential expression (e.g., fold changes). Gene expression values were plotted in various ways (i.e., Scatter, MA, and Volcano plots), using fold-change values, using an R script developed in-house. The protein interaction transfer procedure was performed using the STRING database with the differentially expressed genes. A 60 Gb sequence was generated, and 10,020 transcripts were read and compared. The highest-confidence interaction score (0.9) was applied from the *Mus musculus* species, and information about interacts were obtained based on text mining, experiments, and databases (http://www.string-db.org/).

Reverse transcriptase PCR and real-time PCR

Cells cultured in either 12 or 24-well plates were washed twice with cold PBS and harvested using TaKaRa MiniBEST Universal RNA extraction kit (Takara, Japan). RNA was purified using the same kit according to manufacturer's protocol. RNA was reverse-transcribed using

the cDNA Synthesis Kit (PCRBio Systems, London, UK). Synthesized cDNA was amplified with StepOne Plus (Applied Biosystems, Life Technologies) and 2× qPCRBio Probe Mix Hi-ROX (PCRBio). Comparisons between mRNA levels were performed using the ΔΔCt method, with GAPDH as the internal control.

ELISA and immunoblotting

Mouse TNFα Quantine ELISA kit was purchased from R&D systems (Minneapolis, MN, USA). Raw264.7 cell was seeded at 1 x 10^5 in 12 well cell culture plate and incubated O/N. The cells were then treated with LPS (100ng/ml) and ONG41008 at according concentration. Balancing amount of DMSO was added to each treatment condition. After 24HRs of treatment supernatant from each was collected for ELISA. The assay was performed according to the manufacturer's manual. For three repeat experiment standard curve was made each time to calculate TNFα concentration. For western blotting, antibodies for CD14, MD-2, P62, GAPDH were purchased from Abcam (Cambridge, UK), MyD88, TLR4 from R&D systems, NOX4 (14347-1-AP) from Proteintech (Rosemont, IL, USA), and LC3 A/B, pSMAD-2, pSMAD-3, SMAD2/3, pERK 1/2, ERK 1/2 from Cell Signaling Technology (Danver, MA, USA). All antibodies were diluted to 1:1000 v/v in 5% BSA in DPBS (Welgene).

Immunocytochemistry

Cells were fixed using 4% paraformaldehyde, permeabilized with 0.3% TritonX100, blocked and incubated with 1:500 anti α-Smooth Muscle Actin (Young In Frontier, Korea), 1:500 Actin Phalloidin (Thermo Fisher, USA), 1:500 anti-LTBP1 (Aviva Systems Biology, San Diego, USA), 1:500 anti- LTBP4 (Aviva Systems Biology), 1:500 anti-LAP1 (Abcam), 1:500 anti-integrin α5β3 (biorbyt, Cambridge, UK), 1:500 anti-NOX4 (Proteintech), 1:500 anti-CD14 (Abcam), 1:500 anti-MyD88 (R&D systems), 1:500 anti-TLR4 (R&D systems) or 1:500 anti-

MD-2 (Abcam) antibodies and 1:200 FITC conjugated secondary antibody (Young In Frontier) and imaged with fluorescence microscope EVOS® FL (Thermo). Nuclei were stained with DAPI

Confocal imaging

Cells were fixed with 4% paraformaldehyde, permeabilized with 0.4% Triton X100, blocked with 1% BSA and incubated with anti-CD14 (1:500, Abcam), anti-Myd88 (1:500, R&D systems) for overnight at 4'C. After FITC conjugated secondary antibody incubation (1:200, Ab Frontier) for 1hr at 37'C, images were acquired using Laser scanning confocal microscope (Carl Zeiss LSM700) with 63x oil immersion lens. Confocal images were analyzed with Zen black software.

ROS staining

Intracellular production of ROS was detected after stimulation of ONGHEAPA1 cells with TGFβ (5ng/ml) or TGFβ plus ONG41008 (50uM). Cells were incubated with 10uM H2DCFDA (Abcam) for 1hr in dark at 37'C. The cells were then examined with fluorescence microscope EVOS® FL (Thermo).

Actin polymerization/depolymerization assay

Actin Polymerization/Depolymerization Assay Kit (Abcam, ab239724) was used for both assays. For actin polymerization assay mixture of; actin, buffer, and test samples were placed in 96 plate well in order of supplemented Buffer G (2μM ATP, 5μM DTT), actin, and test samples. As test samples, Buffer G was used as background control, DMSO as positive control, and ONG41008 in DMSO with concentration range from 25 to 100μM were used. The mixtures

in each well were then pipetted thoroughly to mix and incubated in dark, at room temperature, for 15 minutes. After incubation the polymerization activation buffer, supplemented 10X Buffer P (10mM ATP) was added into each well and thoroughly pipetted. For actin depolymerization assay; Buffer G (2μM ATP, 5μM DTT), supplemented 10X Buffer P (10mM ATP), and actin were placed in 96 plate well in listed order and pipetted to mix thoroughly. The mixture was incubated in dark, at room temperature, for 1 hour for polymerization to take effect. After the incubation test samples, DMSO as negative control and ONG41008 at concentration from 25 to 100μM, were added to each appropriate well and pipetted thoroughly. Florescence of both actin polymerization and depolymerization assay were measured with Florescence/Luminescence Analyzer Hidex Sense at florescence Ex/Em 355/405nm (range 5~10nm) in kinetic mode for 2 hours (180 cycles).

Supplemental information

Figure legends

Figure S1. Non-GLP toxicokinetic of ONG41008. (A) ONG41008 was orally administered into mice. Three mice per test group were studied, and their plasma were exercised. (B) Non-GLP single injection oral PK was studied using beagle dogs.

Figure S2. Tissue PK of ONG41008 study. Mice and rat were orally injected ONG41008 at 100mpk. Concentration of drug exposure was detected plasma, lung, liver and kidney tissue at 5min, 15min, 30min, 1hr and 2hr time point.

Figure S3. Tissue PK of ONG41008 study. Mice and rat were orally injected ONG41008 at 100mpk. Concentration of drug exposure was detected plasma, lung, liver and kidney tissue at 5min, 15min, 30min, 1hr and 2hr time point.

Figure S4. Transcriptomic analysis shows 77 TGFβ-induced fibrosis-inducing genes (FIGS) significantly downregulated by ONG41008, including NOX4. (A) Schematic representation of transcriptome selection in treatment of TGFβ and TGFβ plus ONG41008. (B) List of 77 ONG41008 suppressible FIGS. (C) Interactome study using STRING database of listed 77 FIGS. 28 of 77 genes appeared to be isolated from the major interactome. 28 unconnected genes were deleted to better visualize connectivity.

Figure S5. ONG41008 had positive effects against lung fibrosis in both BLM prevention and therapeutic models. (A, C) Lung collagen and hydroxyproline levels measured after

treatment with pirfenidone or 10, 25, or 50 mg/kg ONG41008 in the (A) BLM prevention and (C) BLM therapeutic models. Percent inhibition relative to vehicle control is shown in blue characters, with average measurements in black. (B) Masson's Trichome staining of lung sections in the BLM prevention model. (D) Staining of lung sections with anti-αSMA staining antibody in the BLM therapeutic model. ***P < 0.001, relative to Sham, and $P < 0.05, $$$P < 0.001 relative to vehicle control by Student's t-tests.

Figure S6. Powerful inhibition of LPS-mediated TNFα transcription as well as secreted TNFα (A) CD14 was expressed in plasma membrane of RAW264.7 cell. Nuclei were presented by DAPI (Blue). (B) . Redistribution of CD14 was presented by CD14-LPS binding. RAW264.7cells were stimulated with LPS for 24 hr. (C) The Plasma membrane of RAW264.7 cells stimulated with LPS plus ONG41008 was expressed CD14. RAW264.7 cells were cultured overnight with LPS plus ONG41008. FITC-labeled CD14 (Green) antibody was reacted with RAW264.7 cells. DAPI was used to stain nuclei (blue). The fluorescence of CD14 was detected with 40X objective using EVOS® FL microscope.

Figure S7. The fluorescence levels of MD-2, TLR4, MyD88 and NOX4 was consistent. RAW 264.7 cells were stimulated with Medium, LPS or LPS plus ONG41008 for 24 hr. FITC-labeled Myd88 antibody (1/500), FITC-labeled TLR4 antibody (1/500), FITC-labeled MD-2 antibody (1/500) or FITC-labeled NOX4 antibody (1/500) was immuno-stained with permeabilized RAW 264.7 cells. Nuclei were presented by DAPI (Blue). The image was captured with a 40X objective using EVOS® FL microscope.

Figure S8. The fluorescence levels of MD-2 and NOX4 were unchanging. ICC was conducted as described above. Fluorescence was detected by a fluorescent microscope.

Figure S9. Schematic representation on how ONG4108 would be able to block TLR4 signaling, culminating in production of TNFα and chemokines. A working hypothesis on how ONG41008 markedly affects induction of proinflammatory cytokine, TNFa, and critical immune chemokines such as CCL2, CCL7, CXCL2 and CXCL10. ONG41008 maintains CD14 at periplasmic space, leading to inhibition of endocytosis of CD14. This impairment may be accompanied by blocking endocytosis of Myd88. These combinatorial inability of endcytosis might attenuate intracellular trafficking of TLR4, there by resulting in inactivation of adaptor proteins or transcription factors like IRF family member regulating induction of the above inflammatory cytokines.

Figure S10. Comparison between pirfenidone and ONG41008: inhibitory degree of TGFβ production and lung PK (A) Two-fold difference in molar concentrations between Pirfenidone (185.2) and ONG41008 (470.2) exists. Two drugs exhibited similar degree of *in vivo* TGFβ production at 100 mpk. (B) Calculation basis of presumable mathematical difference in therapeutic efficacy between pirfenidone and ONG41008 considering lung PK: ONG41008 is around (2 X 10=) 20-fold as high as pirfenidone.

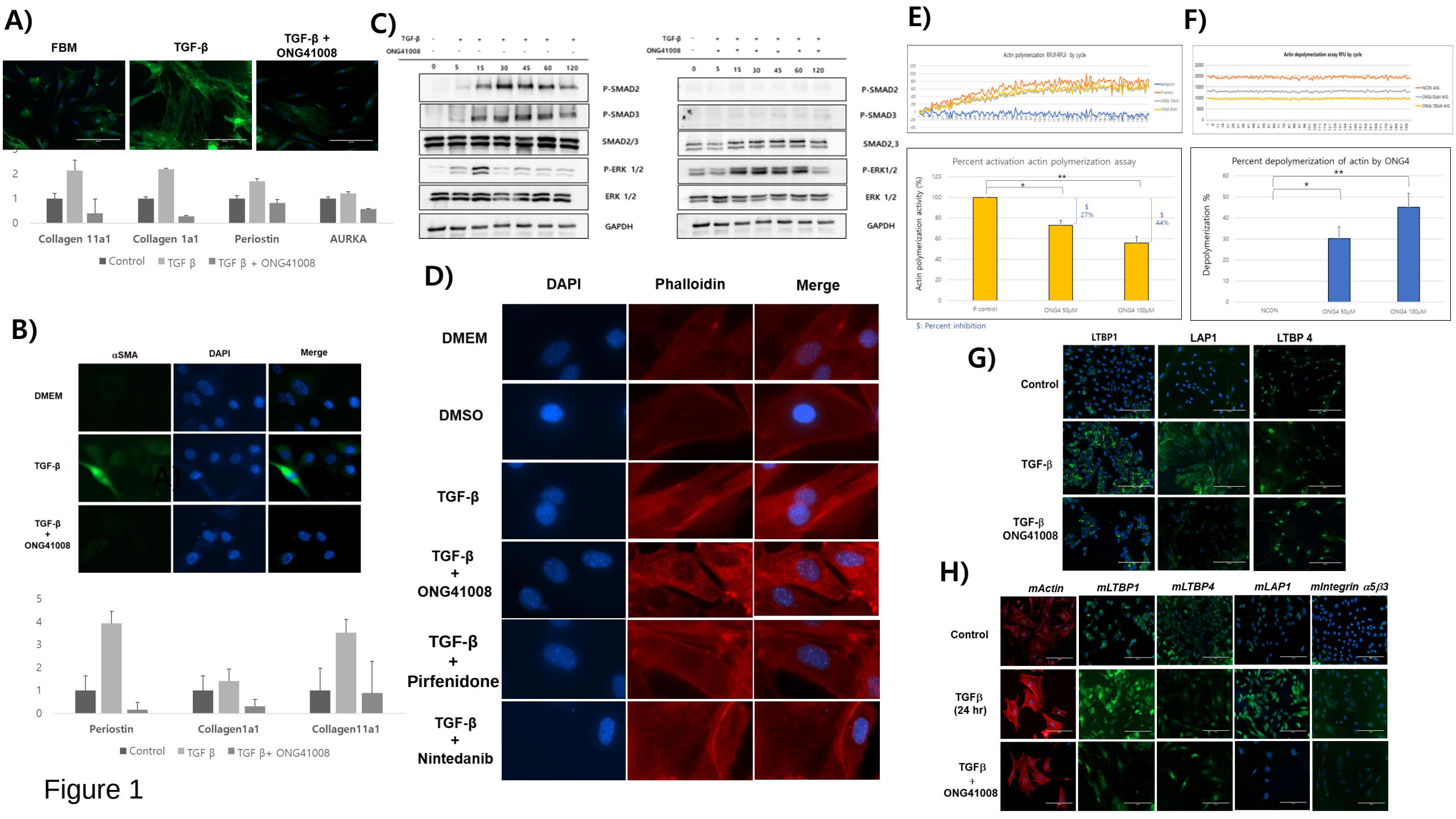
A)
FBM
TGF-β
TGF-β + ONG41008
Collagen 11a1
Collagen 1a1
Periostin
AURKA
Control
TGF β
TGF β + ONG41008
B)
αSMA
DAPI
Merge
DMEM
TGF-β
TGF-β + ONG41008
Periostin
Collagen1a1
Collagen11a1
Control
TGF β
TGF β+ ONG41008
C)
TGF-β
ONG41008
0 5 15 30 45 60 120
P-SMAD2
P-SMAD3
SMAD2/3
P-ERK 1/2
ERK 1/2
GAPDH
SMAD2,3
P-ERK1/2
D)
DAPI
Phalloidin
Merge
DMEM
DMSO
TGF-β
TGF-β + ONG41008
TGF-β + Pirfenidone
TGF-β + Nintedanib
E)
Actin polymerization RFUf-RFUi by cycle
Percent activation actin polymerization assay
Actin polymerization activity (%)
P control
ONG4 50μM
ONG4 100μM
$: Percent inhibition
F)
Actin depolymerization assay RFU by cycle
Percent depolymerization of actin by ONG4
Depolymerization %
NCON
ONG4 50μM
ONG4 100μM
G)
LTBP1
LAP1
LTBP 4
Control
TGF-β
TGF-β ONG41008
H)
mActin
mLTBP1
mLTBP4
mLAP1
mIntegrin α5β3
Control
TGFβ (24 hr)
TGFβ + ONG41008

Figure 1

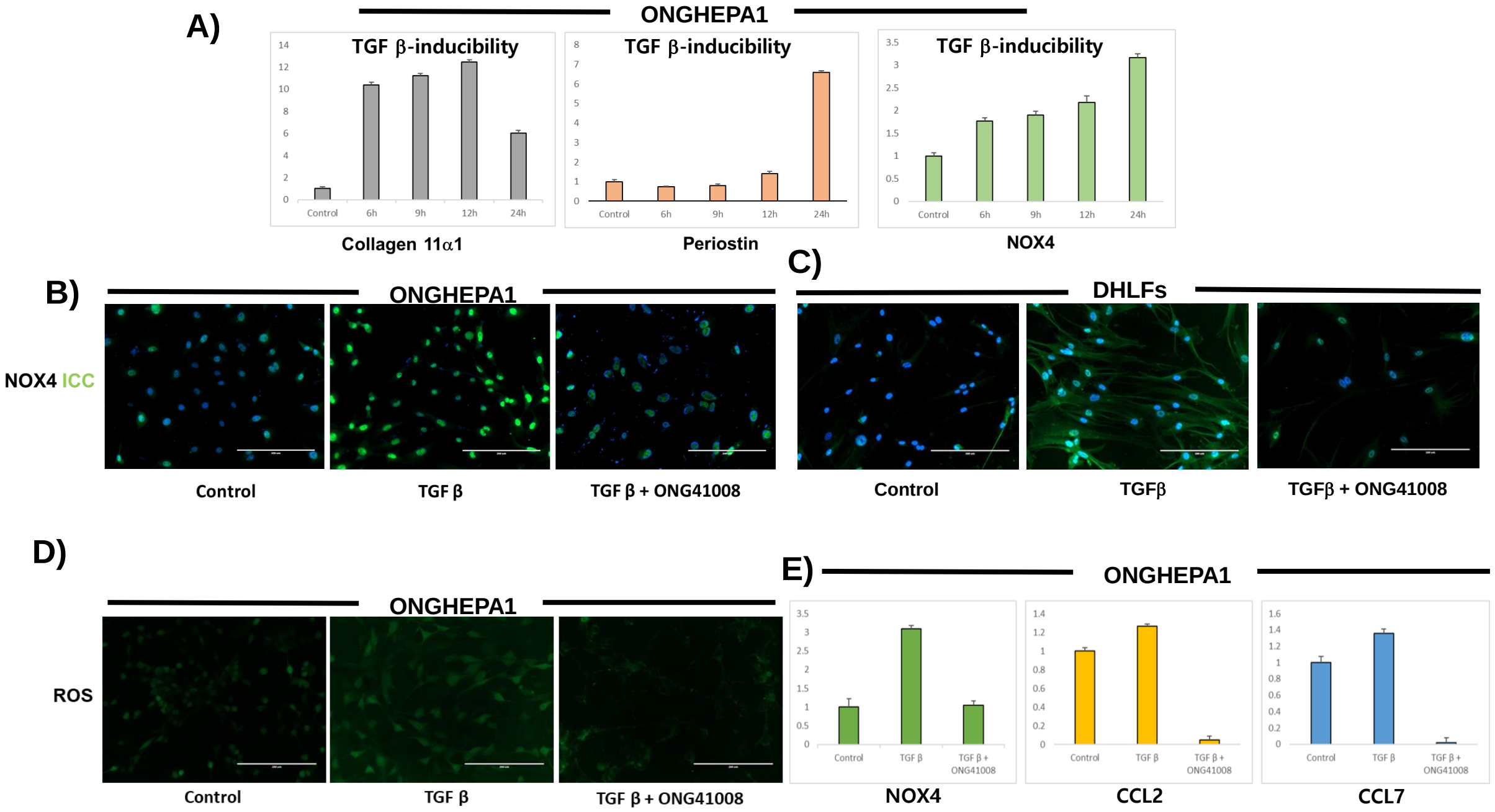
A)
ONGHEPA1
TGF β-inducibility
Control
6h
9h
12h
24h
Collagen 11α1
Periostin
NOX4
B)
ONGHEPA1
NOX4 ICC
Control
TGF β
TGF β + ONG41008
C)
DHLFs
Control
TGFβ
TGFβ + ONG41008
D)
ONGHEPA1
ROS
Control
TGF β
TGF β + ONG41008
E)
ONGHEPA1
Control
TGF β
TGF β + ONG41008
NOX4
CCL2
CCL7

Figure 2

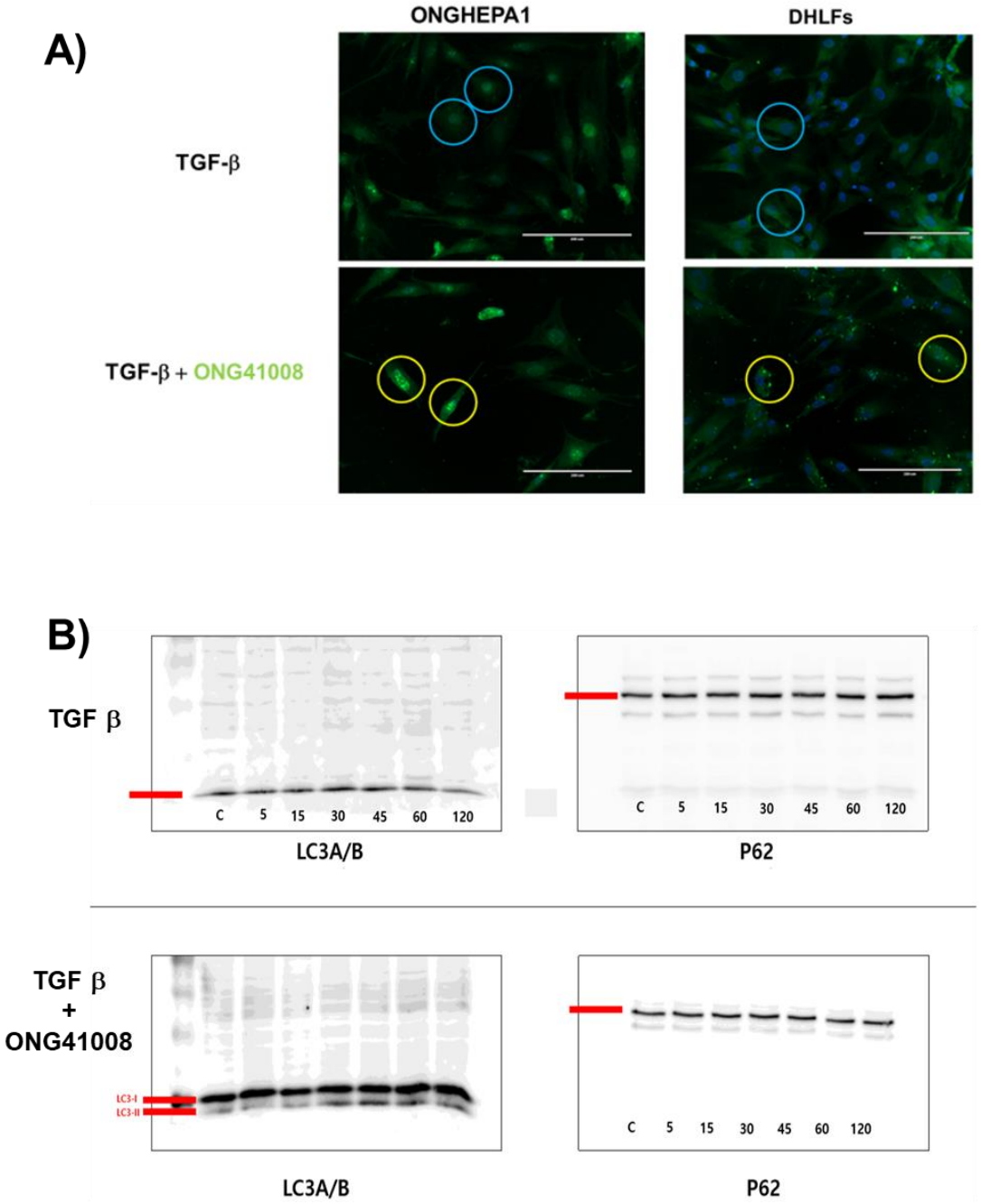
A)
ONGHEPA1
DHLFs
TGF-β
TGF-β + ONG41008
B)
TGF β
C 5 15 30 45 60 120
LC3A/B
C 5 15 30 45 60 120
P62
TGF β
+
ONG41008
LC3-I
LC3-II
LC3A/B
C 5 15 30 45 60 120
P62

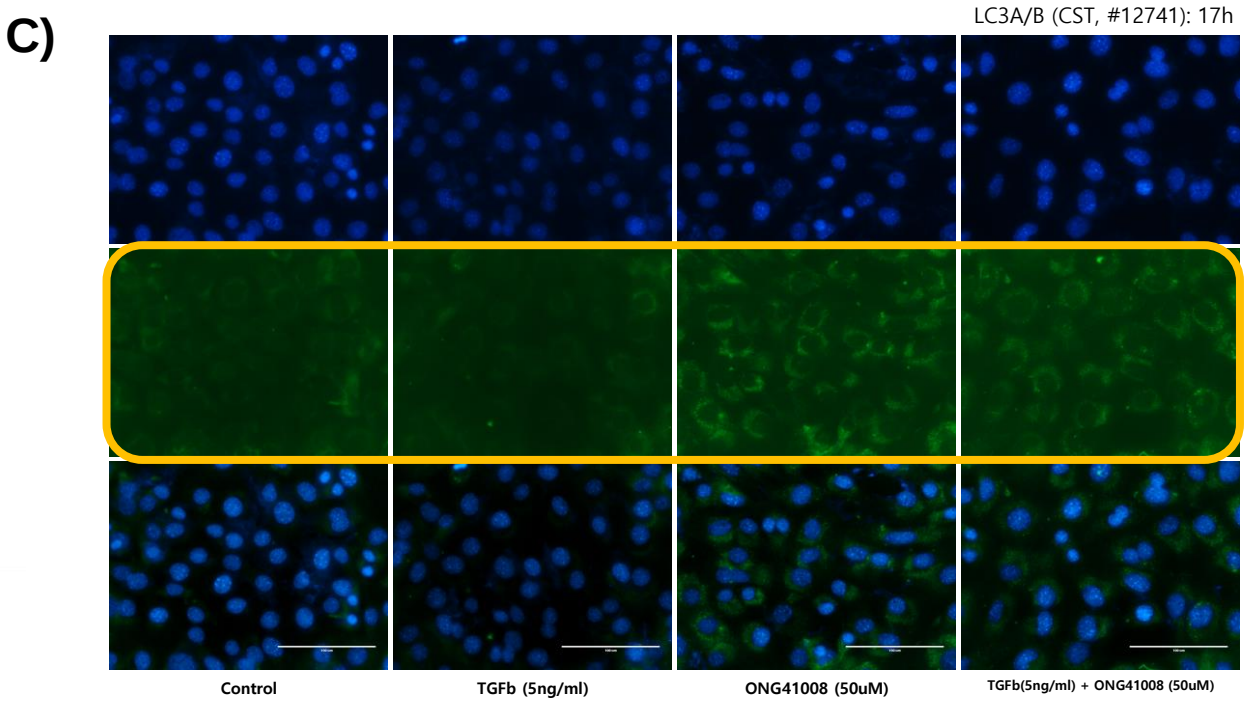
C)
LC3A/B (CST, #12741): 17h
Control
TGFb (5ng/ml)
ONG41008 (50uM)
TGFb(5ng/ml) + ONG41008 (50uM)

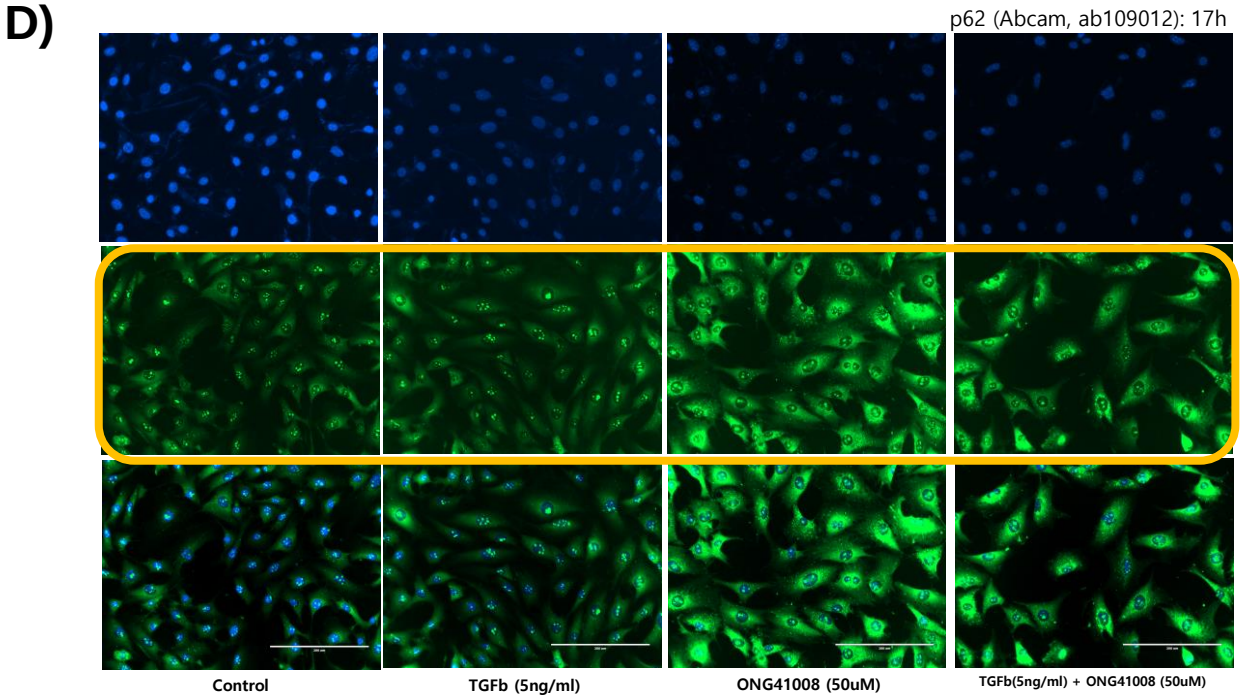
D)
p62 (Abcam, ab109012): 17h
Control
TGFb (5ng/ml)
ONG41008 (50uM)
TGFb(5ng/ml) + ONG41008 (50uM)

Figure. 3

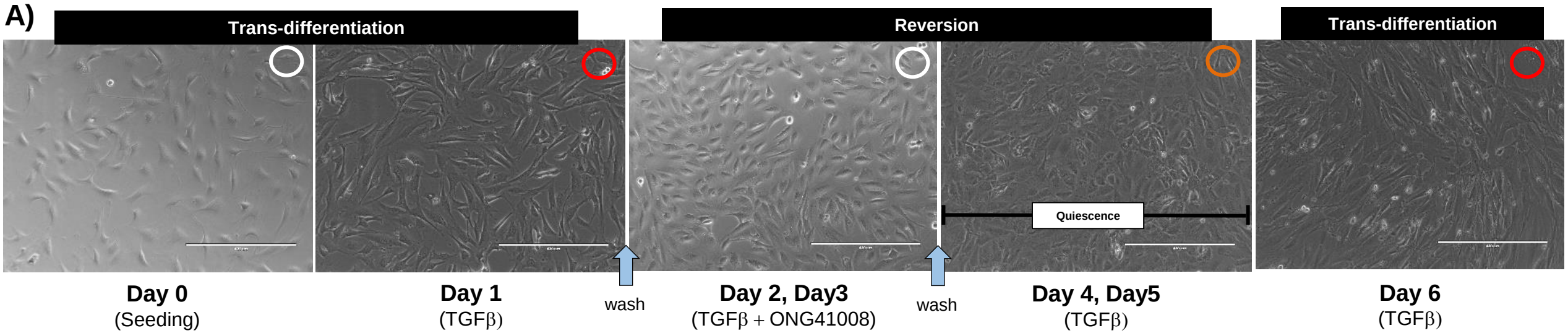
A)
Trans-differentiation
Reversion
Trans-differentiation
Quiescence
Day 0
(Seeding)
Day 1
(TGFβ)
wash
Day 2, Day3
(TGFβ + ONG41008)
wash
Day 4, Day5
(TGFβ)
Day 6
(TGFβ)

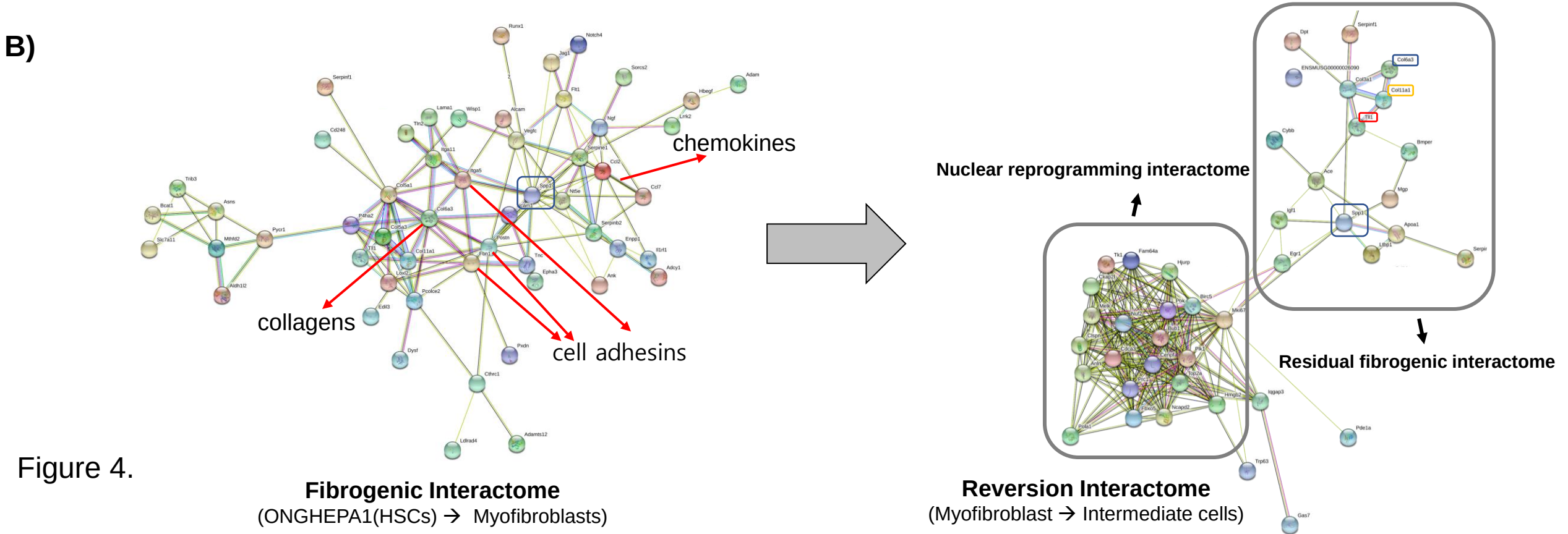
B)
chemokines
collagens
cell adhesins
Nuclear reprogramming interactome
Residual fibrogenic interactome
Fibrogenic Interactome
(ONGHEPA1(HSCs) → Myofibroblasts)
Reversion Interactome
(Myofibroblast → Intermediate cells)

Figure 4.

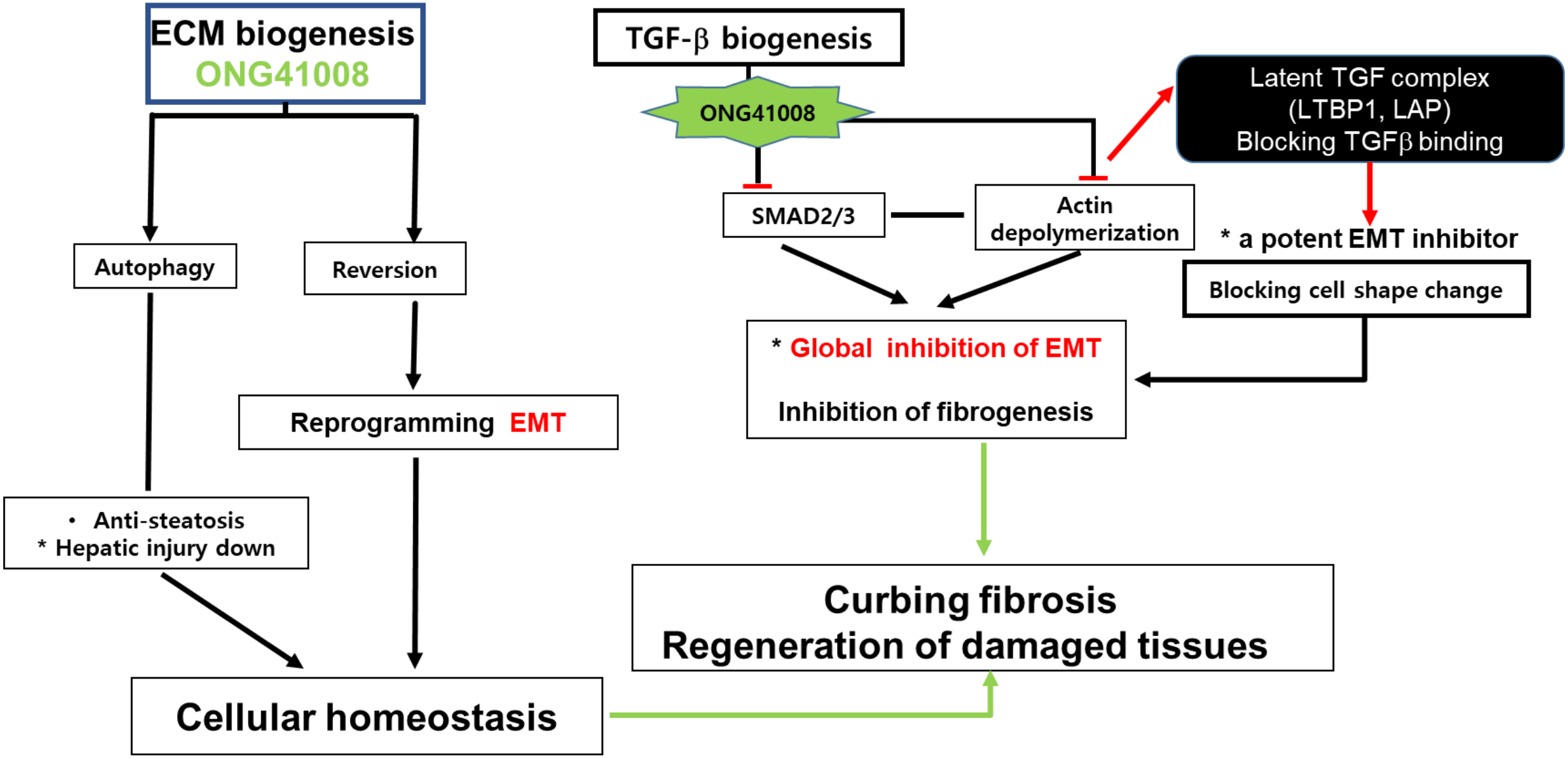
ECM biogenesis
ONG41008
Autophagy
Reversion
Reprogramming EMT
• Anti-steatosis
* Hepatic injury down
Cellular homeostasis
TGF-β biogenesis
ONG41008
SMAD2/3
Actin depolymerization
Latent TGF complex
(LTBP1, LAP)
Blocking TGFβ binding
* a potent EMT inhibitor
Blocking cell shape change
* Global inhibition of EMT
Inhibition of fibrogenesis
Curbing fibrosis
Regeneration of damaged tissues

Figure. 5

A) BLM therapeutic model

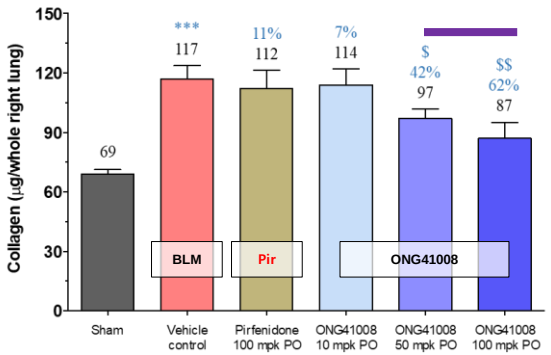

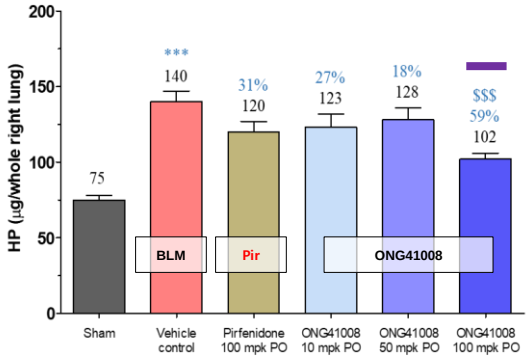

B) *αSMA* staining

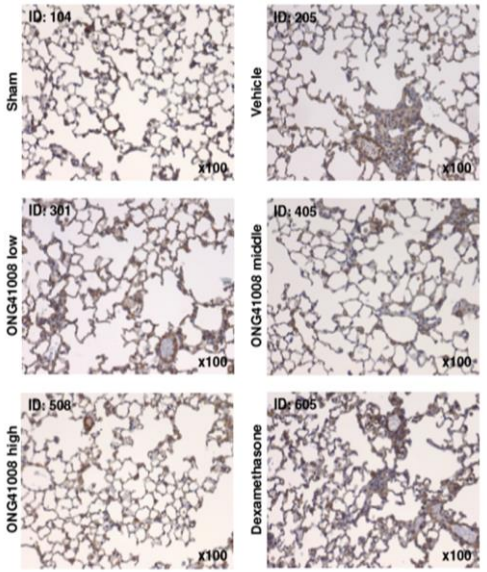

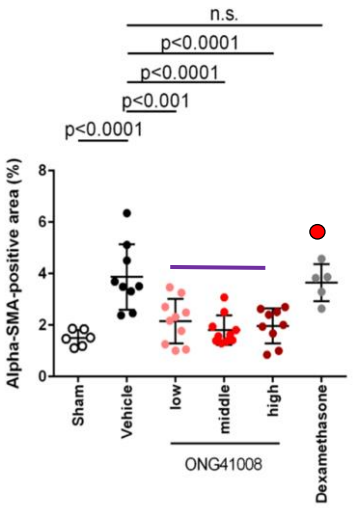

Low: ONG41008 10mpk
Middle: ONG41008 25mpk
High: ONG41008 50mpk
Dexamethasone 0.25mpk

C)

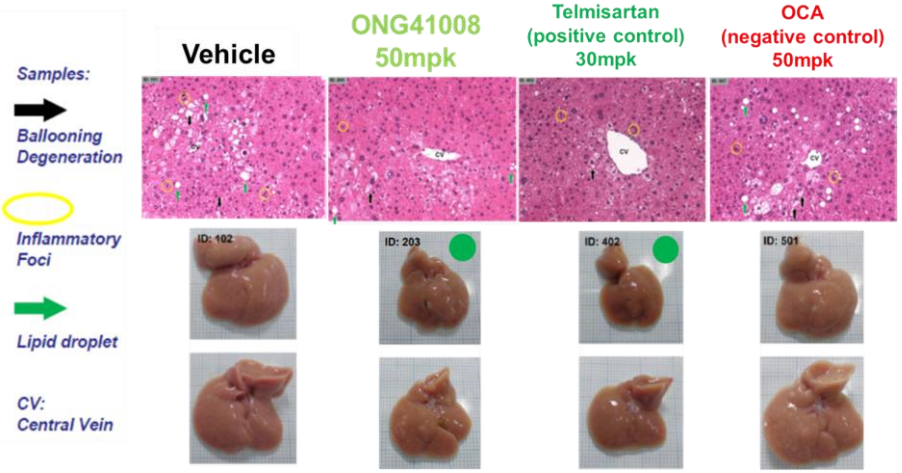

D)

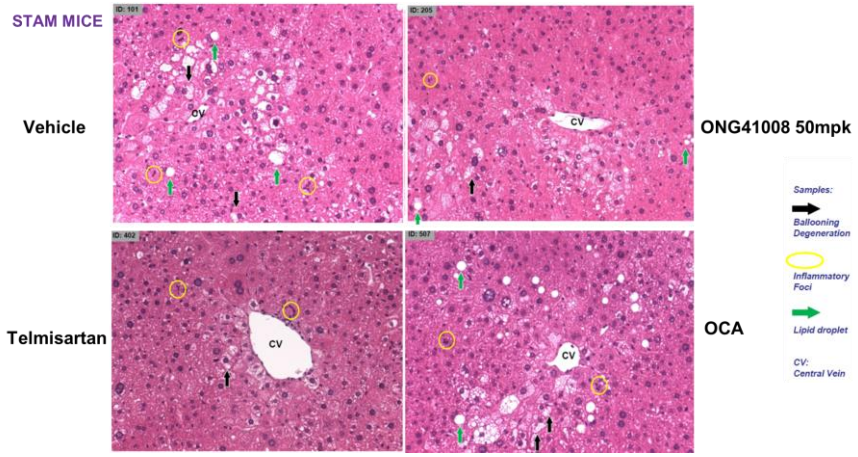

E)

Group	n	Score											NAS (mean ± SD)
		Steatosis				Lobular inflammation				Hepatocyte ballooning			
		0	1	2	3	0	1	2	3	0	1	2	
Vehicle	8	3	5	-	-	-	-	2	6	1	5	2	4.5 ± 0.8
ONG41008	6	3	3	-	-	-	1	2	3	3	2	1	3.5 ± 0.8
Telmisartan	7	5	2	-	-	-	1	5	1	2	4	1	3.1 ± 1.2
OCA	8	3	5	-	-	-	-	6	2	2	4	2	3.9 ± 1.1

Definition of NAS Components

Item	Score	Extent
Steatosis	0	<5%
	1	5-33%
	2	>33-66%
	3	>66%
Lobular Inflammation	0	No foci
	1	<2 foci/200x
	2	2-4 foci/200x
	3	>4 foci/200x
Hepatocyte Ballooning	0	None
	1	Few balloon cells
	2	Many cells/prominent ballooning

F)

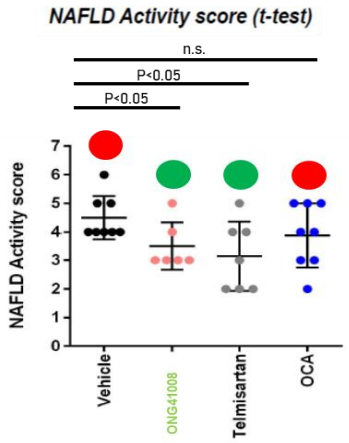

Figure 6

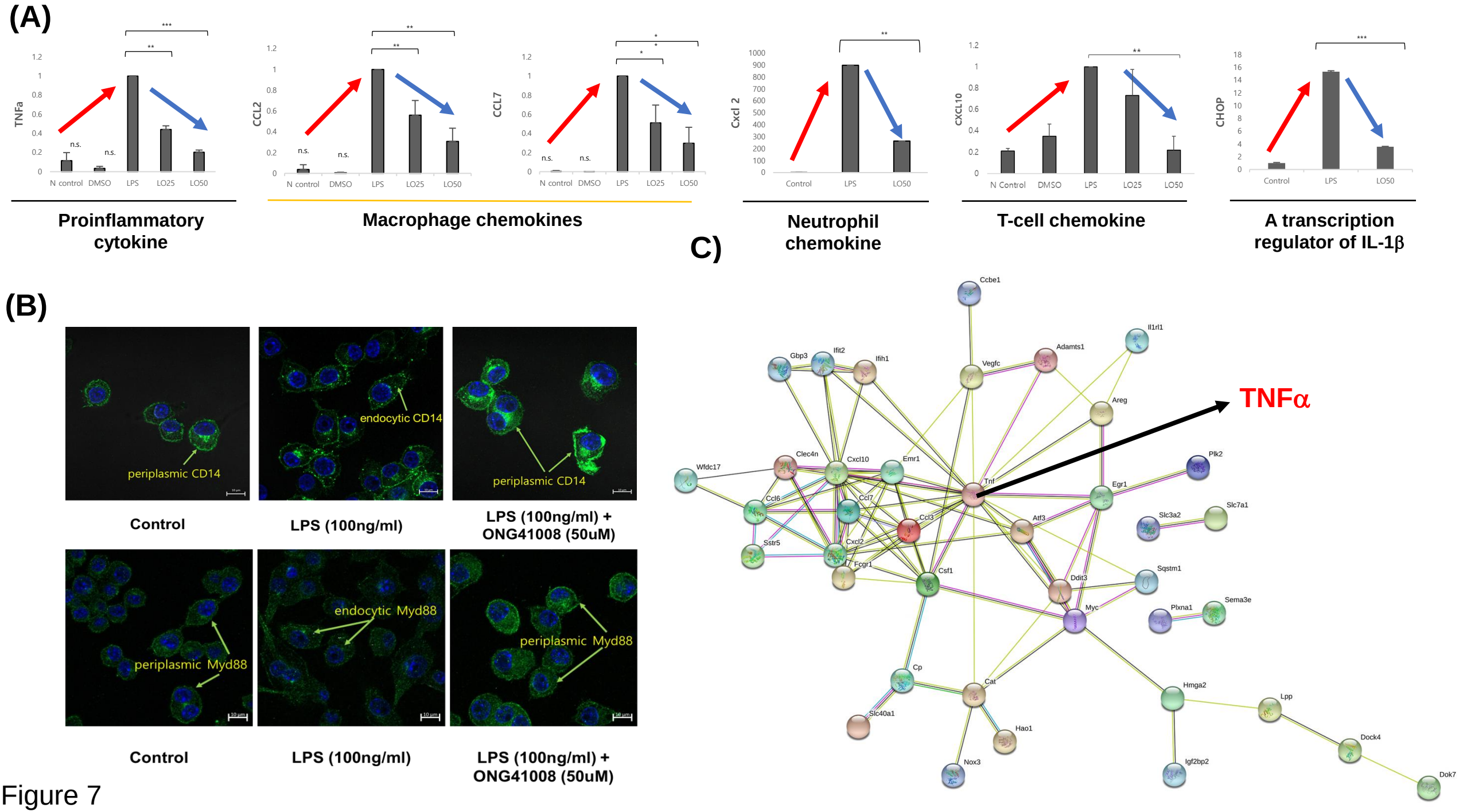
(A)
TNFa
CCL2
CCL7
Cxcl 2
CXCL10
CHOP
N control
DMSO
LPS
LO25
LO50
N Control
Control
n.s.
Proinflammatory cytokine
Macrophage chemokines
Neutrophil chemokine
T-cell chemokine
A transcription regulator of IL-1β
(B)
periplasmic CD14
endocytic CD14
periplasmic CD14
Control
LPS (100ng/ml)
LPS (100ng/ml) + ONG41008 (50uM)
periplasmic Myd88
endocytic Myd88
periplasmic Myd88
Control
LPS (100ng/ml)
LPS (100ng/ml) + ONG41008 (50uM)
C)
TNFα
Ccbe1
Il1rl1
Adamts1
Vegfc
Gbp3
Ifit2
Ifih1
Areg
Plk2
Wfdc17
Clec4n
Cxcl10
Emr1
Tnf
Egr1
Ccl6
Ccl7
Ccl3
Atf3
Slc3a2
Slc7a1
Sstr5
Cxcl2
Fcgr1
Csf1
Ddit3
Sqstm1
Sema3e
Plxna1
Myc
Cp
Cat
Hmga2
Lpp
Slc40a1
Hao1
Dock4
Nox3
Igf2bp2
Dok7

Figure 7